Check for updates

JOURNAL OF QUATERNARY SCIENCE (2024) 1–12 ISSN 0267-8179. DOI: 10.1002/jqs.3687

JQS Journal of Quaternary Science QRA Quaternary Research Association

Pre-Marine Isotope Stage 2 glacial activity around the Nevado de Chañi massif in the Central Andes of Argentina and paleoclimate implications

MATEO A. MARTINI,[1]* MICHAEL R. KAPLAN,[2] LUCIA GUERRA,[1] ESTABAN SAGREDO,[3,4] JOERG M. SCHAEFER[2,5] and MARC W. CAFFEE[6,7]

[1]Centro de Investigaciones en Ciencias de la Tierra (CONICET-UNC), Facultad de Ciencias Exactas, Físicas y Naturales, Universidad Nacional de Córdoba, Córdoba, Argentina
[2]Lamont-Doherty Earth Observatory of Columbia University, Palisades, NY, USA
[3]Instituto de Geografía, Pontificia Universidad Católica de Chile, Santiago, Chile
[4]Estación Patagonia de Investigaciones Interdisciplinarias UC, Pontificia Universidad Católica de Chile, Chile
[5]Department of Earth and Environmental Sciences, Columbia University, New York, NY, USA
[6]Department of Physics and Astronomy, Purdue University, West Lafayette, IN, USA
[7]Department of Earth, Atmospheric, and Planetary Science, Purdue University, West Lafayette, IN, USA

Received 5 June 2024; Revised 9 October 2024; Accepted 8 December 2024

ABSTRACT: We describe and analyze the glacial geomorphology and new ^{10}Be cosmogenic surface exposure ages from moraines deposited before Marine Isotope Stage (MIS) 2 around Nevado de Chañi (24°4′ S, 65°45′ W), a north–south-trending massif located in the arid subtropical mountains of northwestern Argentina. We combine these data with previously published ages in order to establish a glacier chronology around the massif and the central Andes. The results show at least three phases of glacier expansions occurred before the global Last Glacial Maximum, (i) during MIS 6, (ii) close to the transition from MIS 4 to MIS 3, and (iii) during mid-late MIS 3. Based on a comparison of the timing of glacier advances with other glacial and paleoclimatic proxies elsewhere, we infer that glaciers grew in this arid region of the subtropical Andes during periods of reduced temperatures and wetter conditions, ultimately due to intensification of the South American Summer Monsoon. In contrast, during MIS 5 no glacial activity was recorded around the massif, and we infer that even if wetter conditions prevailed in the region the temperature was not sufficiently low to support glaciations. © 2024 John Wiley & Sons, Ltd.

KEYWORDS: cosmogenic dating; geomorphology; glaciations; moraines; South America; subtropics

Introduction

Mountain glaciers, such as in the central Andes, are sensitive to changes in climate, particularly temperature, precipitation, and the amount of solar (shortwave) radiation received at high and dry elevations (Sagredo and Lowell, 2012; Mackintosh et al., 2017; Olson and Rupper, 2019). Glaciogenic deposits and landforms are critical elements to unravel past climate changes since they represent direct proxies of glacier fluctuations. In the Central and Tropical Andes (Fig. 1), different analyses on lake sediment records have been used to infer past changes in glacier mass balance and activity in the high mountain ranges (Baker et al., 2001; Fritz et al., 2007; Woods et al., 2020; Rodbell et al., 2022). They record alternating glacial and interglacial climate conditions since the Middle Pleistocene, in consonance with the fluctuations of δ^{18}O benthic foraminiferal stack from deep-sea sediment cores, a proxy for changes in Northern Hemisphere ice volume (Lisiecki and Raymo, 2005). Nevertheless, information regarding mountain glacier fluctuations and their chronology, particularly prior to Marine Isotope Stage (MIS) 2 (29–14 ka), is scarce, especially for findings that directly record glacier advances and retreats (e.g. Ward et al., 2015; Zech et al., 2017). Studies of the timing and extent of the former glaciers in the high mountains of the Central Andes are critical to understand past climate changes in this understudied region. Such efforts will also permit confirmation of mountain glacier activity inferred from complementary but indirect proxies (e.g. lake sediments).

The Last Glacial Maximum (LGM) is considered as the period of maximum ice-sheet and glacier extension during the last glacial cycle (~110–10 ka). Different approaches have been used to establish its temporal extent, and most of them overlap with the first half of MIS 2 (e.g. Mix et al., 2001; Hughes and Gibbard, 2015; Hughes, 2022). Based on a review of mountain glaciers and ice-sheet chronologies around the world together with sea-level records, Clark et al. (2009) defined the global LGM interval between ~26.5 and 19 ka. Nevertheless, it has been recognized that some mountain glaciers all over the world reached their last maximum extent in different moments prior to MIS 2 (Gillespie and Molnar, 1995; Denton et al., 2021).

Regardless of definition, the global LGM (26.5–19 ka; cf. Clark et al., 2009) and the subsequent last termination, over most of MIS 2, have been the target of many works along the Central Andes (e.g. Bromley et al., 2016; Martin et al., 2020; Palacios et al., 2020). Consequently, major progress has been made in understanding the nature and causes that drove glacial expansions during MIS 2. Comparatively, less is known regarding mountain glacier activities prior to MIS 2, because the glacial record is usually fragmented and therefore it is difficult to establish absolute chronologies. Moreover, the preservation of pre-MIS 2 glacial deposits (e.g. moraines) is often limited because younger, larger glacier advances can erode the older deposits, resulting in a gap in the record. Arid regions offer an opportunity to study pre-global LGM glaciations since post-depositional erosional processes are usually

*Correspondence: Mateo A. Martini, as above.
E-mail: mmartini@unc.edu.ar

© 2024 John Wiley & Sons, Ltd.

less effective in erasing completely or disturbing glacial landforms. Cosmogenic surface exposure dating provides an opportunity to establish robust chronologies that pre-date the last glacial cycle (e.g. Leger et al., 2023), filling gaps in the current knowledge of pre-MIS 2 glaciations. Such studies are lacking in the Central Andes.

In this study, we focus on the Nevado de Chañi (24°S), located immediately north of the Arid Diagonal and under the domain of the South American Summer Monsoon (SASM). The massif contains an abundant record of Late Pleistocene glacial deposits. As elsewhere, the chronological efforts have thus far tended to focus on MIS 2 and the last termination (Martini et al., 2017a; Mey et al., 2020), with older glacial deposits being studied in less detail. Here, we map, characterize and present a new set of ^{10}Be ages from the pre-global LGM moraines around Nevado de Chañi. We combine our results with published data to analyze the paleoclimatic context and mechanisms that drove glacier activity in the region.

Study area

Regional setting

The Nevado de Chañi is located on the Cordillera Oriental of northwestern Argentina (Fig. 1). It is a north–south mountain range that separates the arid Puna-Altiplano to the west and the subtropical lowland rainforest to the east. The massif has its highest peak at 5940 m asl and contains many others that exceed 5500 m asl. It is mainly composed of Precambrian and Lower Paleozoic metasedimentary rocks and sandstones intruded by Cambrian granites (Gonzalez et al., 2004; Zappetini et al., 2008). Notable geomorphological and climatic differences exist between the east and west sides of the massif. On the east side, the climate is wetter, and the terrain has steeper slopes and higher relief, produced in part by glacial erosion and fluvial incision, than in the western area (Figs. 2–4). Commonly, periglacial features such as active rock glaciers lie at the foot of cirques and headwalls on the eastern side, whereas on the western side these features are scarce (Martini et al., 2013). The regional altitude of the 0°C isotherm (freezing level) is estimated at ~5000 m (Martini et al., 2017b). Although the Nevado de Chañi comprises a large area above the freezing level no glaciers exist around the massif because of the extreme conditions prevailing in the area, which include a combination of a low amount of precipitation, high solar radiation and intense wind.

The Nevado de Chañi is located immediately north of the Arid Diagonal, a band of low precipitation (<250 mm a^{-1}) that crosses South America with a northwest–southeast orientation (Fig. 1). At present, the climate in the area is mainly controlled by the SASM and its components. During the beginning of the austral spring, the Intertropical Convergence Zone moves southward and produces the onset of the SASM (Zhou & Lau 1998; Vera et al., 2006; de Carvalho & Cavalcanti, 2016) which reaches its mature phase between December and March when more than 70% of the annual precipitation is concentrated around Nevado de Chañi (Bianchi & Yañez, 1992). During this time, a deep continental low forms over the Chaco region (25°S) and forces the easterly winds to turn southward and transport significant amounts of moisture through the South American Low Level Jet from the Amazon region into northwestern Argentina (Garreaud et al., 2009; cf., 'monsoon-like' conditions). The air trajectory is from the east and northeast which generates a steep orographic precipitation regime on the east side of the Cordillera Oriental (Bianchi and Cravero, 2010; Viale et al., 2019). At 2000 m asl precipitation is 1600 mm a^{-1}, and above 3500 m asl, where the evidence of former glacier expansions is present, arid conditions prevail (total annual precipitation decreases to <400 mm). In the highest sectors of Nevado de Chañi, snowfall is frequent during the summer, but its presence on the ground is short (typically less than a few days) due to the high daily temperature prevailing during this season.

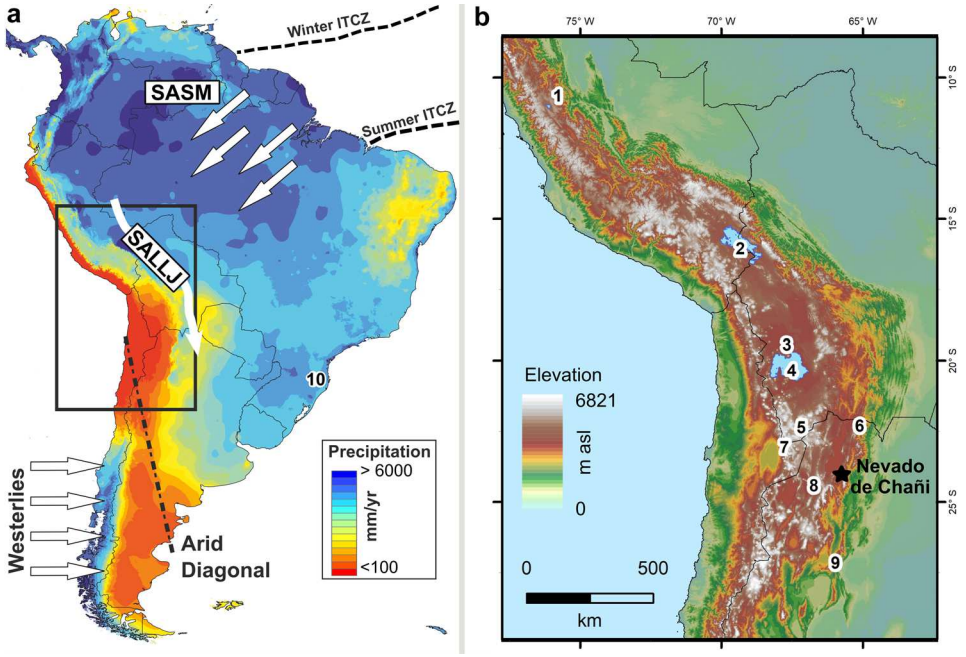

Figure 1. Regional setting. (a) Precipitation map of South America (WorldClim database; Hijmans et al., 2005). Arrows denote the wind and moisture trajectory. The dashed lines over the ocean mark the position of the Inter Tropical Convergence Zone (ITCZ) in the Atlantic Ocean during the austral winter and summer. SASM: South American Summer Monsoon; SALLJ: South American Low Level Jet. (b) Digital Elevation Model of the Central Andes. Numbers represent sites mentioned in the text. 1: Junin Lake (Rodbell et al., 2022), 2: Lake Titcaca (Fritz et al., 2007), 3: Tunupa volcano (Blard et al., 2009), 4: Salar de Uyuni salt-lake (Fritz et al., 2004), 5: Uturuncu volcano (Blard et al., 2014), 6: Tres Lagunas (Zech et al., 2009), 7: Chajnantor Plateau (Ward et al., 2015), 8: Quevar volcano (Luna et al., 2018), 9: Sierra de Aconquija (D'Arcy et al., 2019), 10: Botuverá cave (Cruz et al., 2005). [Color figure can be viewed at wileyonlinelibrary.com]

© 2024 John Wiley & Sons, Ltd.

10991417, 0, Downloaded from https://onlinelibrary.wiley.com/doi/10.1002/jqs.3687 by Columbia University Health Sciences, Wiley Online Library on [14/01/2025]. See the Terms and Conditions (https://onlinelibrary.wiley.com/terms-and-conditions) on Wiley Online Library for rules of use; OA articles are governed by the applicable Creative Commons License

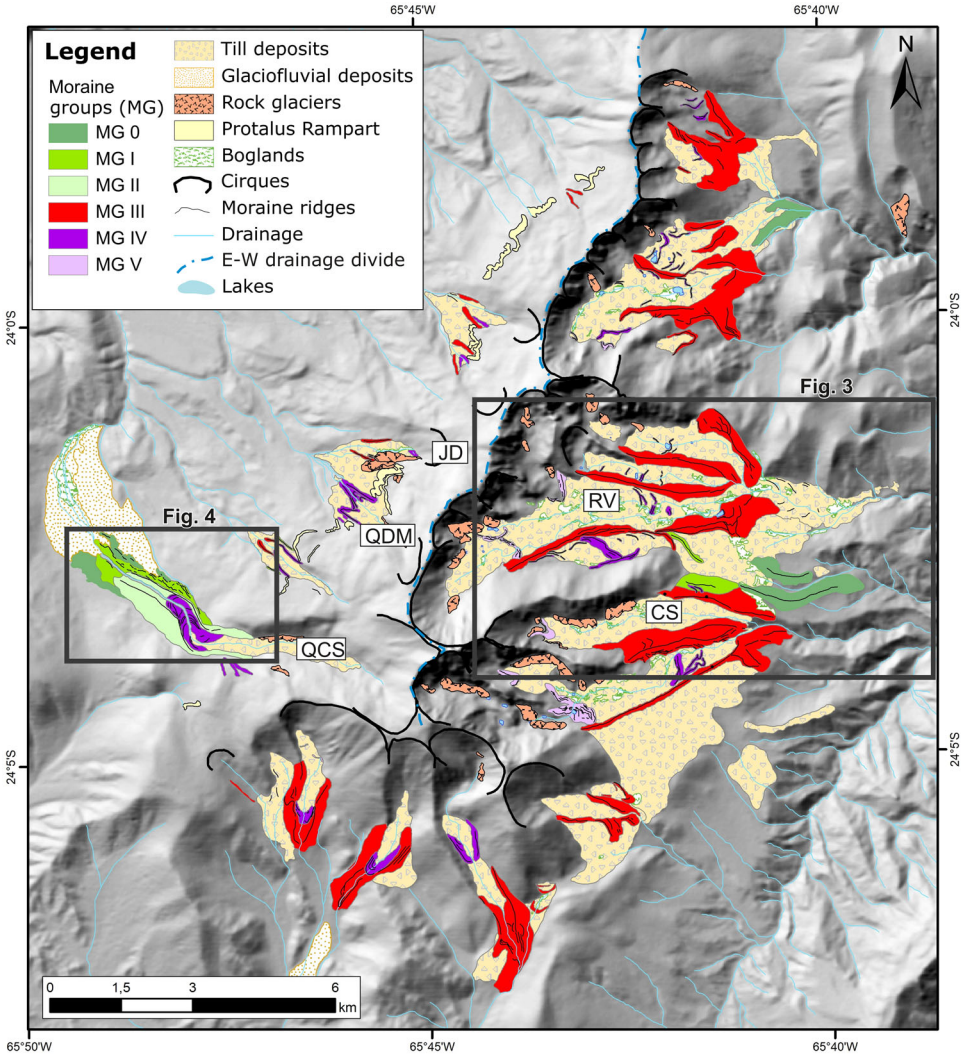

Figure 2. Glacial geomorphologic map of the Nevado de Chañi massif. Note that the glacial geomorphology is better developed on the east side (see 'Glacier chronology'). JD: Jefatura de Diablos valley; QDM: Quebrada del Medio valley; QCS: Quebrada de Chañi Sur valley; CS: Chañi Sur valley; RV: Refugio valley. [Color figure can be viewed at wileyonlinelibrary.com]

Existing glacier chronology around Nevado de Chañi

Nevado de Chañi features several valleys formerly occupied by glaciers draining mainly to the east and west of the massif. Martini et al. (2017a) divided the moraine record of Nevado de Chañi into five different moraine groups (MGs). From oldest to youngest, they were named MG I, II, III, IV and V. Martini et al. (2017a) dated 42 boulders on moraine crests using ^{10}Be cosmogenic surface exposure dating. Dated samples were from the Refugio valley on the east side, and from Jefatura de Diablos, Quebrada de la Mina and Chañi sur valleys on the west side (Fig. 2).

MG I and MG II were dated only on the west side at ~60–40 ka ($n = 3$) and 45–40 ka ($n = 3$), respectively (Martini et al., 2017a). MG III represents an important glacier advance on the east side at 21–25 ka, during the global LGM ($n = 10$); it is poorly represented or lacking on the west side. MG IV was interpreted as a stillstand or minor glacial advance, which is well represented on both sides of Nevado de Chañi, occurring at ~15 ka ($n = 12$). Finally, upward from MG IV, and only represented in the east side, MG V was dated at ~12–13 ka ($n = 4$). During the last glacial termination, the glacial chronology of Nevado de Chañi roughly matches with stadials recorded in the Northern Hemisphere, specifically during Heinrich stadial 1 (MG IV) and the Younger Dryas (MG V). Mey et al. (2020) added 20 new ^{10}Be ages on moraines, focusing on the global LGM and last glacial termination on both sides of Nevado de Chañi, reinforcing the chronology obtained by Martini et al. (2017a).

According to Martini et al. (2017a), glacier activity around Nevado de Chañi during the global LGM and the last termination was controlled largely by changes in precipitation, as well as temperature. The reconstructed paleo-equilibrium line altitudes suggest an eastward moisture trajectory during the MIS 2 glacial events (Martini et al., 2017a). Using numerical models, Mey et al. (2020) quantified past temperature and precipitation changes. They found that temperatures were between 2.0–3.3 and 1.3–2.5°C lower and precipitation increased by 9–46 and 13–50 mm a^{-1} during Heinrich stadial 1 and Younger Dryas, respectively. During the last termination, the similarity of SASM proxies and glacial expansions around Nevado de Chañi suggest that similar forcing factors may have controlled their activity (Martini et al., 2017a).

Methods

Glacial geomorphologic mapping

We mapped the geomorphology focusing on the pre-MIS 2 glacial deposits around the Nevado de Chañi massif, building on that in Martini et al. (2017a) (Fig. 2) and Mey et al. (2020).

© 2024 John Wiley & Sons, Ltd.

10991417, 0, Downloaded from https://onlinelibrary.wiley.com/doi/10.1002/jqs.3687 by Columbia University Health Sciences, Wiley Online Library on [14/01/2025]. See the Terms and Conditions (https://onlinelibrary.wiley.com/terms-and-conditions) on Wiley Online Library for rules of use; OA articles are governed by the applicable Creative Commons License

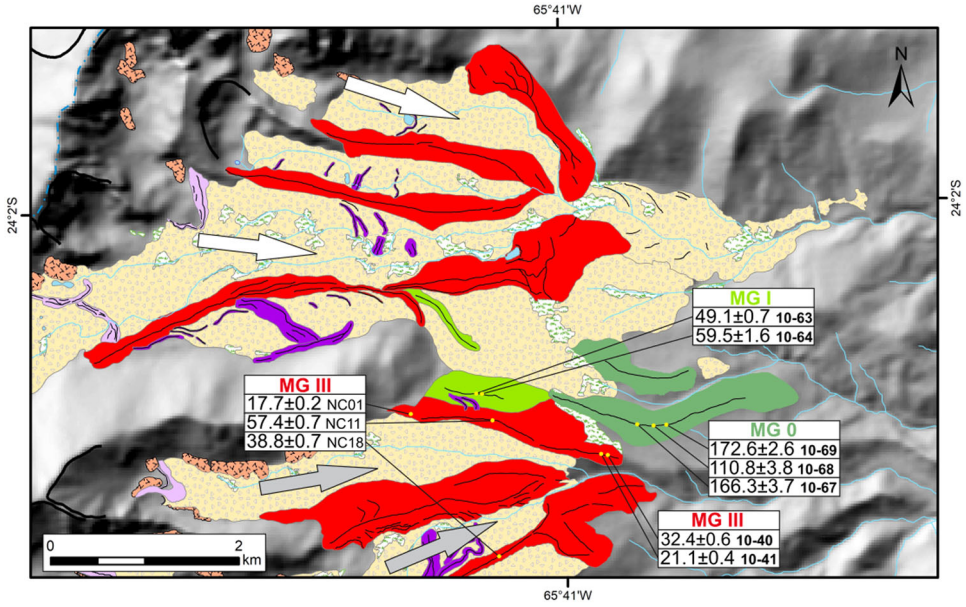

Figure 3. Detailed glacial geomorphologic map of the Refugio and Chañi Sur valleys on the east side of Nevado de Chañi. Yellow dots are locations of boulders dated using ^{10}Be. Ages are presented inside boxes in ka ('Lm' scaling) and ±1σ analytical (internal) uncertainty. Sample ID (last four digits) is shown in smaller front (in bold, samples presented in this study; Table 2). White and gray arrows represent the former glacier flow direction in the Refugio and Chañi Sur valleys, respectively. Refer to Fig. 2 for geomorphologic key and location. Other ^{10}Be ages in Martini et al. (2017a) and Mey et al. (2020) for MG IV and V, and MG for the Refugio valley mainly associated with MIS 2, are not shown. [Color figure can be viewed at wileyonlinelibrary.com]

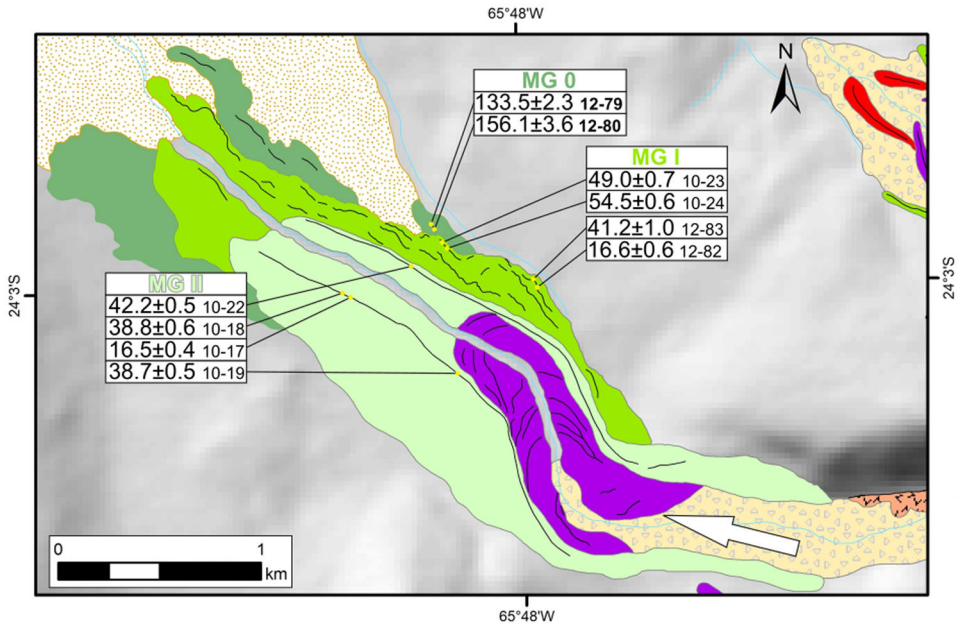

Figure 4. Detailed glacial geomorphologic map of the Quebrada de Chañi Sur valley area on the west side of Nevado de Chañi. Yellow dots are locations of boulders dated using ^{10}Be. Ages are presented inside boxes in ka ('Lm' scaling) and ±1σ analytical (internal) uncertainty. Sample ID (last four digits) is shown in smaller front (in bold, samples presented in this study; Table 2). The white arrow represents the former glacier flow direction. Refer to Fig. 2 for geomorphologic key and location. Other ^{10}Be ages in Martini et al. (2017a) for MG IV are not shown. [Color figure can be viewed at wileyonlinelibrary.com]

We used high-resolution satellite imagery, aerial photographs and ALOS PALSAR digital elevation models to produce a glacial geomorphologic map of the area. Fieldwork was conducted to check the interpretations based on remote sensing and to collect rock samples for ^{10}Be dating. We focused the mapping and sampling activities on the Quebrada de Chañi sur valley on the west side of Nevado de Chañi, and the Refugio and Chañi Sur valleys on the east side (Figs. 2–4). Based on the geomorphology and chronology of the glacial deposits, we separated the morainic deposits into MGs following the classification of Martini et al. (2017a).

Surface exposure ^{10}Be cosmogenic dating

We sampled nine boulders deposited atop moraine crests for ^{10}Be dating. We chose big (≥1 m tall) granitic boulders grounded in the moraine to avoid post-depositional disturbance (e.g. boulder rotation or exhumation) (Fig. 5). The samples were taken from the top 2–3 cm of horizontal and flat boulder surfaces using a hammer and chisel. For each sample, we described the boulder, its geomorphological context and the surface of sampling, and measured their shielding using a compass and clinometer. The location and altitude of each sample were measured using differential Global Navigation

© 2024 John Wiley & Sons, Ltd.

10991417, 0, Downloaded from https://onlinelibrary.wiley.com/doi/10.1002/jqs.3687 by Columbia University Health Sciences, Wiley Online Library on [14/01/2025]. See the Terms and Conditions (https://onlinelibrary.wiley.com/terms-and-conditions) on Wiley Online Library for rules of use; OA articles are governed by the applicable Creative Commons License

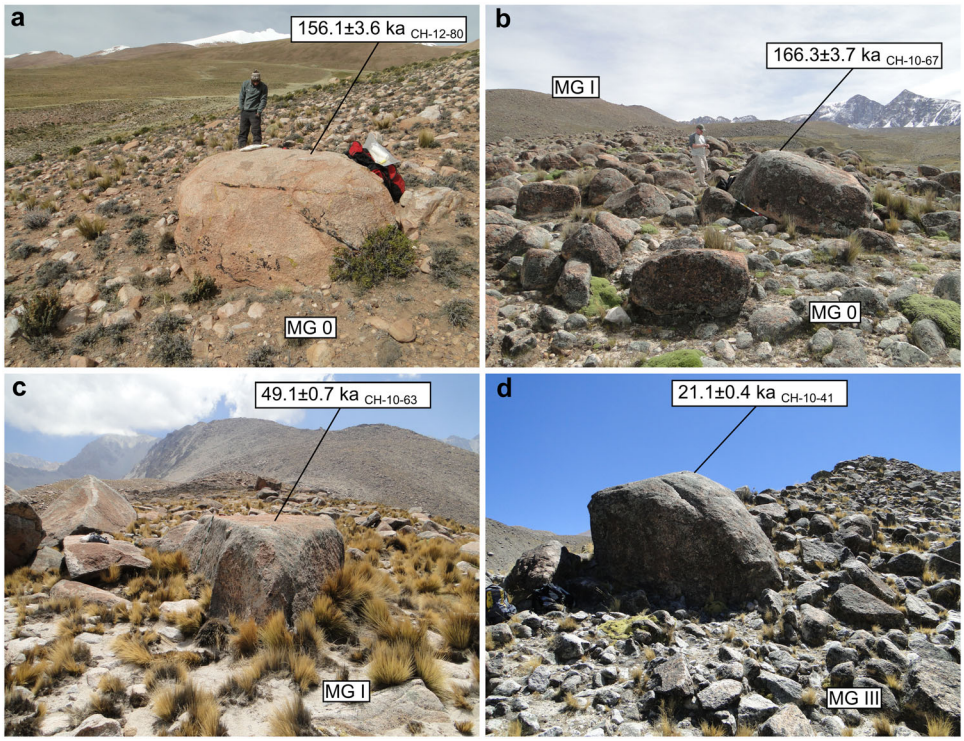

Figure 5. Examples of boulders dated using ^{10}Be including their age in ka ('Lm' scaling) and ±1σ, sample ID, and geomorphological context around Nevado de Chañi. (a) Large erratic boulder of MG 0 on the west side. (b) Subdued moraines of MG 0 on the east side. In the background is MG I. (c) MG I on the east side. (d) Lateral/frontal moraine of MG III on the east side. MG: moraine group. [Color figure can be viewed at wileyonlinelibrary.com]

Table 1. Geographic and analytical ^{10}Be cosmogenic sample data. ^{10}Be concentrations are corrected for ^{10}Be in process blanks run with each sample batch.

Sample ID	Latitude (°S)	Longitude (°W)	Altitude (m asl)	Boulder height (m)	Sample thickness (cm)	Shielding correction	^{10}Be (atoms g^{-1})	±1σ ^{10}Be (atoms g^{-1})	MG
CH-10-67[a]	−24.05423	−65.67568	4126	1.4	1.0	0.998	7657 129	165 373	0
CH-10-68[a]	−24.05418	−65.67399	4097	1.7	1.0	0.999	5015 161	165 160	0
CH-10-69[a]	−24.05421	−65.67267	4077	2.1	1.2	0.999	7720 976	111 161	0
CH-12-79[b]	−24.04730	−65.80410	4435	1.0	0.6	0.998	7277 183	123 342	0
CH-12-80[b]	−24.04750	−65.80400	4442	1.0	0.8	0.998	8415 039	184 271	0
CH-10-63[a]	−24.05151	−65.69236	4500	1.5	3.2	0.998	2576 692	34 581	I
CH-10-64[a]	−24.05159	−65.69221	4498	2.1	0.7	0.998	3059 959	83 404	I
CH-10-40[a]	−24.05734	−65.67878	4145	1.3	1.2	0.997	1443 991	24 740	III
CH-10-41[a]	−24.05716	−65.67949	4170	2.3	1.0	0.997	903 161	18 566	III

MG: moraine group. *Blank ^{10}Be atoms (±1σ): 5206 ± 4089. †Blank ^{10}Be atoms (±1σ): 9341 ± 6227.

Satellite System. We interpret the ^{10}Be ages from moraine boulders on crest tops as dating relatively close to the end of the causal climate event or close to the onset of withdrawal of the ice margin from the landform.

^{10}Be extraction from whole rock was carried out in the Cosmogenic Nuclide Laboratory at the Lamont-Doherty Earth Observatory of Columbia University following the methods described in Schaefer et al. (2009). ^{10}Be/^{9}Be ratios were measured at PRIME Lab relative to the 07KNSTD accelerator mass spectrometry standard (Nishiizumi et al., 2007). During the chemical procedures we used a blank for each batch of samples (n = 9-12) and the ^{10}Be concentration of the blank was subtracted from the sample's measurement to remove background ^{10}Be. In all cases the blank corrections represent less than 0.12% of the sample measurement. Analytical data are shown in Table 1.

^{10}Be ages were calculated using the online exposure age calculator (version 3, https://hess.ess.washington.edu/math/v3/v3_age_in.html; Balco et al., 2008), assuming no erosion (as we purposely avoided clear evidence of this, and samples are of resistant lithologies), a rock density of 2.65 g cm^{-3} and no snow shielding due to the low precipitation of the region (e.g. Martini et al., 2017b). We used the high-altitude low-latitude regional production rate (3.78 ± 0.09 at g^{-1}a^{-1}) of Kelly et al. (2015) and show the time-dependent 'Lm' scaling. Production rate uncertainty is 2.4% (Kelly et al., 2015), which is well within the range or variability of ages. We note that using the other regional production rate (i.e. Martin et al., 2015) the ages vary by less than 1%. In addition, we discuss ^{10}Be ages derived with the 'LSD' scaling, which tends to be between 5 and 8% older than that with 'Lm'. Nevertheless, the choice of scaling or production rate does not affect the major interpretations and conclusions of this study. For previously published ^{10}Be cosmogenic ages, we followed the same procedures to recalculate the ages.

Results

Moraine groups (MG)

Based on the mapping and chronological results, we distinguish three moraine groups (MG) constructed beyond the

© 2024 John Wiley & Sons, Ltd.

10991417, 0, Downloaded from https://onlinelibrary.wiley.com/doi/10.1002/jqs.3687 by Columbia University Health Sciences, Wiley Online Library on [14/01/2025]. See the Terms and Conditions (https://onlinelibrary.wiley.com/terms-and-conditions) on Wiley Online Library for rules of use; OA articles are governed by the applicable Creative Commons License

global LGM moraines limit (i.e. MG III): MG 0, MG I and MG II (Figs. 2–4). MG 0 is the only moraine group that was not previously reported by Martini et al. (2017a).

MG 0 is the most expanded margin, and it is recognized on both sides of the massif. In the Quebrada de Chañi Sur valley, on the west side, it is represented by subdued discontinuous moraine ridges, which are better preserved on the northeast side of the valley (Fig. 5a). Due to the preserved lateral/frontal moraines, it is possible to mark the maximum extent of the advance that generated MG 0 in Quebrada de Chañi Sur. On the east side, MG 0 is represented by lateral moraines generated by glaciers that flowed from the Refugio and the Chañi Sur valleys (Fig. 5b). The deposits consist of subdued ridges that extend down to ~3800 m asl and contain large erratic boulders. The distance that this glacial expansion reached on the east side is unknown since frontal moraines are not preserved. Erratic boulders of granite can be tracked, at least, until 3400–3500 m asl suggesting that this glacial expansion extended to these altitudes.

In the Quebrada de Chañi Sur valley, MG I is partially overridden by MG II, which is the most prominent MG in the valley with sharp lateral moraines more than 50 m in height (Fig. 4). On the east side, we revisited the MG I and MG II complexes and some of the previous mapping and interpretations (Martini et al., 2017a), based on the new geomorphological evidence and ^{10}Be ages presented in this work. MG I is composed of lateral moraines present in the north and south sectors of the Chañi Sur and Refugio valleys, respectively. The Chañi Sur valley lateral moraine is more restricted and at a higher elevation than the lateral moraine in the Refugio valley. Both moraines exhibit subdued topography and are topped by large granitic boulders (Fig. 5c). MG II was not identified on the east side of Nevado de Chañi.

The glacier record of Nevado de Chañi during the global LGM is represented by MG III, which consists of sharp well-preserved lateral and frontal moraines on the east side of the massif (Fig. 5d). The lateral/frontal MG III moraines in the Refugio and Chañi Sur valleys attain more than 70 m in height and are located above 4000 m asl, representing an important glacier event recorded in both valleys. In turn, on the western side of the massif, in the Quebrada de Chañi valley we have not recognized moraines that could match with MG III (Fig. 4). Finally, smaller moraines located inboard (MG IV and V) represent younger glacial events (outside the scope of this study and discussed in prior papers: Martini et al., 2017a; Mey et al., 2020) (Fig. 2).

^{10}Be surface-exposure dating

We present nine new ^{10}Be ages. In addition, we re-calculate eight ^{10}Be ages in Martini et al. (2017a) and three in Mey et al. (2020) (Tables 1 and 2), all of which correspond to MG 0, I, II and III landforms.

Five ^{10}Be ages date the MG 0 limits. Three ages are from a lateral moraine of the Chañi Sur paleoglacier on the east side (172.6 ± 2.6, 166.3 ± 3.7 and 110.8 ± 3.8 ka) and the other two are from a lateral moraine in the Quabrada de Chañi sur valley on the west side (156.1 ± 3.6 and 133.5 ± 2.3 ka) (Figs. 3–5 and Table 2).

Two new samples from MG I on the east side of Nevado de Chañi afford ages of 59.5 ± 1.6 and 49.1 ± 0.7 ka (Figs. 3 and 5). The two samples are situated on a lateral moraine in the Chañi Sur valley, which is located 200 m above the dated lateral moraine of the previously deposited MG 0 limit. On the west side, four recalculated ages for MG I from Martini et al. (2017a) are 54.5 ± 0.6, 49.0 ± 0.7, 41.2 ± 1.0 and 16.6 ± 0.6 ka.

For MG II, four ^{10}Be ages recalculated from Martini et al. (2017a), from the Quebrada de Chañi Sur valley on the west side, yield ages of: 42.2 ± 0.5, 38.8 ± 0.6 38.7 ± 0.5 and 16.5 ± 0.4 ka (Table 2). Finally, we obtained two new ages (32.4 ± 0.6 and 21.1 ± 0.4 ka) from the frontal moraine of MG III in the Chañi Sur valley, which complement three ages reported by Mey et al. (2020) (57.4 ± 0.7, 38.8 ± 0.7 and 17.7 ± 0.2 ka) (Fig. 3).

Discussion

Glacier chronology

The new set of ages presented here provide insight into past glaciations in the Central Andes and South America prior to

Table 2. ^{10}Be surface exposure ages and internal uncertainty from Nevado de Chañi (see Figs. 3 and 4). Ages are shown using the local production rate of Kelly et al. (2015) with the time-dependent 'Lm' and LSD scaling (Balco et al., 2008).

	Lm		LSD			
Sample ID	Age (ka)	Internal uncertainty (ka)	Age (ka)	Internal uncertainty (ka)	MG	Source
CH-10-67	166.3	3.7	179.7	4.1	0	This study
CH-10-68*	110.8	3.8	117.3	4.0	0	This study
CH-10-69	172.6	2.6	184.7	2.8	0	This study
CH-12-79	133.5	2.3	142.2	2.5	0	This study
CH-12-80	156.1	3.6	167.5	3.8	0	This study
CH-10-63	49.1	0.7	53.0	0.7	I	This study
CH-10-64	59.5	1.6	62.1	1.7	I	This study
CH-10-40*	32.4	0.6	35.1	0.6	III	This study
CH-10-41	21.1	0.4	22.2	0.5	III	This study
CH-10-23	49.0	0.7	53.1	0.7	I	Martini et al. (2017a)
CH-10-24	54.5	0.6	57.7	0.6	I	Martini et al. (2017a)
CH-12-82*	16.6	0.6	17.5	0.6	I	Martini et al. (2017a)
CH-12-83*	41.2	1.0	43.1	1.0	I	Martini et al. (2017a)
CH-10-17*	16.5	0.4	17.4	0.4	II	Martini et al. (2017a)
CH-10-18	38.8	0.6	40.6	0.7	II	Martini et al. (2017a)
CH-10-19	38.7	0.5	40.5	0.5	II	Martini et al. (2017a)
CH-10-22	42.2	0.5	44.6	0.5	II	Martini et al. (2017a)
NC01*	17.7	0.2	18.7	0.3	III	Mey et al. (2020)
NC11*	57.4	0.7	60.3	0.8	III	Mey et al. (2020)
NC18*	38.8	0.7	40.5	0.8	III	Mey et al. (2020)

MG: moraine group. Samples marked with an asterisk (*) next to the sample ID are considered outliers.

© 2024 John Wiley & Sons, Ltd.

10991417, 0, Downloaded from https://onlinelibrary.wiley.com/doi/10.1002/jqs.3687 by Columbia University Health Sciences, Wiley Online Library on [14/01/2025]. See the Terms and Conditions (https://onlinelibrary.wiley.com/terms-and-conditions) on Wiley Online Library for rules of use; OA articles are governed by the applicable Creative Commons License

MIS 2. They complement and build on chronologies in prior works around Nevado de Chañi (Martini et al., 2017a; Mey et al., 2020). In some cases, ^{10}Be ages are not consistent with other samples in the same moraine group or on crests. It is possible that inconsistent ages do not represent the timing of moraine formation, and instead reflect pre-exposure (inheritance) or boulder disturbance after deposition, as we discuss in this section.

A total of five samples are from the MG 0 limit: three from the east side and two from the west side of the massif. The two oldest ages from the east side overlap at 2σ, whereas the ^{10}Be age of 110.8 ± 3.8 ka is much younger (by >60 kyr) than the other two, possibly reflecting post-depositional disturbance and it does not represent the timing of moraine deposition (i.e. an outlier). On the west side, MG 0 samples were taken from a small lateral moraine ridge in the Quebrada de Chañi Sur valley and the ages are 156.1 ± 3.6 and 133.5 ± 2.3 ka (Figs. 4 and 5). Given these ages are overall younger than those from the east side (172.6 ± 2.6 and 166.3 ± 3.7 ka), the MG 0 landforms from the east and west sides could represent two different (instead of one unique) glacial events, with the former slightly older. Nevertheless, the younger age from the east side (166.3 ± 3.7 ka) and the older age from the west side (156.1 ± 3.6 ka) just overlap if ±2σ is considered. Given this is the most expanded glacial event registered as landforms around Nevado de Chañi, and the number of ages obtained, we tentatively assign MG 0 on both sides of the massif to the same general glaciation between ~173 and ~134 ka. Perhaps the ~134 ka age reflects the structure (i.e. more than one event) within the MIS 6 glaciation of the region, which remains to be tested with additional data. We note that age differences between the west and east sides are unlikely to be due to cosmogenic nuclide systematics, as production rate and scaling are essentially identical. Last, we note that if LSD scaling is used the ages range from 168–142 ka (west side) to 185–180 ka (east side).

Excluding one outlier (16.6 ± 0.6 ka), the MG I ages range from 59.5 ± 1.6 to 41.2 ± 1.0 ka ($n = 5$). We note that the youngest age (41.2 ± 1.0 ka) overlaps with those of MG II (see below) and is more than 7 kyr younger than the other four samples from MG I (Figs. 3 and 4). It is possible that this boulder has moved or rotated after deposition (there is no apparent evidence of erosion), and we tentatively suggest that it does not represent the MG I depositional age. Combining the east and west side samples for MG I, the age of deposition ranges from ~59 to ~49 ka ($n = 4$). If LSD scaling is used the ages of MG I increase by 6% and range from ~62 to ~52 ka. Regarding MG II, three ages from the west side (excluding one outlier, 16.5 ± 0.4 ka, perhaps reflecting post-depositional disturbance), of 42.2 ± 0.5, 38.8 ± 0.6 and 38.7 ± 0.5 ka, form a coherent cluster. Therefore, the MG II age (only dated on the west side) ranges from ~42 to ~39 ka ($n = 3$; 45–40 ka using LSD scaling).

Inboard of MG 0 and I, the MG III in the Chañi Sur valley exhibit five different ^{10}Be ages that range between 57.4 ± 0.7 and 17.7 ± 0.2 ka, without a clear cluster (Fig. 3). We note that one of the ages (38.8 ± 0.7 ka) matches with the MG II chronology on the west side, and therefore the interpreted MG III on the Chañi Sur valley could be part of the MG II event. Nevertheless, based on the geomorphology, setting in the valley and mapping, we correlate this moraine group with the well-dated lateral and frontal moraines of MG III in the Refugio valley, which are constrained in age to between 21 and 25 ka ($n = 10$, Martini et al., 2017a), that is during the global LGM (26.5–19 ka, cf. Clark et al., 2009). Considering this interpretation, the age of 21.1 ± 0.4 ka may indicate the true MG III depositional age. The older ages could be affected by ^{10}Be inheritance, similar to other samples that exhibit considerably older ages compared with the main cluster of results from MG III landforms in the Refugio valley (Martini et al., 2017a; Mey et al., 2020). More data are needed to corroborate these assumptions and compare the two valleys in detail.

The glacial record around Nevado de Chañi exhibits an asymmetry between the east and west side of the massif (Figs. 2–4), in geomorphologic expression and dated events. Some inferences regarding the moisture trajectory can be made based on this asymmetry in glacier coverage (and erosion) and spatial changes in glacier equilibrium line altitudes (Martini et al., 2017a; Mey et al., 2020). Although the glacial deposits have been partially eroded on the east side and therefore the frontal moraines are not preserved, the paleogeography is still revealed for pre-MIS 2 glacier coverage. The MIS 6 moraines (MG 0) reach lower elevations and extend farther from the drainage divide on the east compared to the west side. This can be explained by the eastward source of moisture, ultimately from the Atlantic, that facilitates more precipitation and perhaps less ablation (i.e. when cloudy; Garreaud et al., 2009) and a lower equilibrium line altitude on the east side. On the east side, during the formation of MG I and II related inferences are not possible based on geomorphology alone since MG III partially eroded the former and possibly all of the latter MG II. This implies that the MG III event corresponding to the global LGM was relatively more important on the east side compared to the west side, although the MG III chronology in the Chañi Sur valley (east side) can be better constrained.

Comparison with other glacier and paleoclimate records

The Nevado de Chañi massif has a rich history of former glacier activity that extends back to at least ~170 ka and is represented by six or more main periods of moraine construction. Before the global LGM, which is locally represented by MG III, at least three distinct glacial expansions are still preserved. The oldest (MG 0) took place during MIS 6 (191–130 ka; Lisiecki and Raymo, 2005) at ~174–134 ka. Afterwards, successively less extensive glacier expansions are dated close to the transition from MIS 4 to 3 and slightly after, ~59–49 ka (MG I), and during MIS 3 between ~42 and ~39 ka (MG II, only dated on the west side). As we assume ages may be close to the end of the moraine building phase (see 'Surface exposure ^{10}Be cosmogenic dating'), those that overlap statistically with the end of MIS 4 may reflect this global glaciation (Doughty et al., 2021). The glacier chronology presented links the interpretations to the large-scale (>multi-millennial) paleoclimatic changes that occurred in South America since MIS 6, which can be compared with regional and global paleoclimate proxies. The matches with global and regional events (see next section) are not dependent on cosmogenic ^{10}Be scaling and production rate chosen (Table 2).

The oldest and most extended glacier expansion, dated to ~173–134 ka (MG 0), occurred before the last glacial cycle, and was in phase with high Northern Hemisphere ice volume throughout MIS 6 (Lisiecki and Raymo, 2005) and low temperatures in the high latitudes of the Southern Hemisphere (EPICA, 2004) (Fig. 6). Evidence for other glacial advances in the central Andes during MIS 6 comes from the Tunupa volcano in the Bolivian Altiplano (20°S; Blard et al., 2009) and with less confidence in the Tres Lagunas area (Cordillera Oriental, 22°S; Zech et al., 2009), Quevar massif (Puna, 24°S; Luna et al., 2018) and Chajnantor Plateau (Chilean Altiplano, 23°S; Ward et al., 2015) (Fig. 1). MIS 6 glacier expansions, also larger than those during MIS 2, are documented in the

© 2024 John Wiley & Sons, Ltd.

10991417, 0, Downloaded from https://onlinelibrary.wiley.com/doi/10.1002/jqs.3687 by Columbia University Health Sciences, Wiley Online Library on [14/01/2025]. See the Terms and Conditions (https://onlinelibrary.wiley.com/terms-and-conditions) on Wiley Online Library for rules of use; OA articles are governed by the applicable Creative Commons License

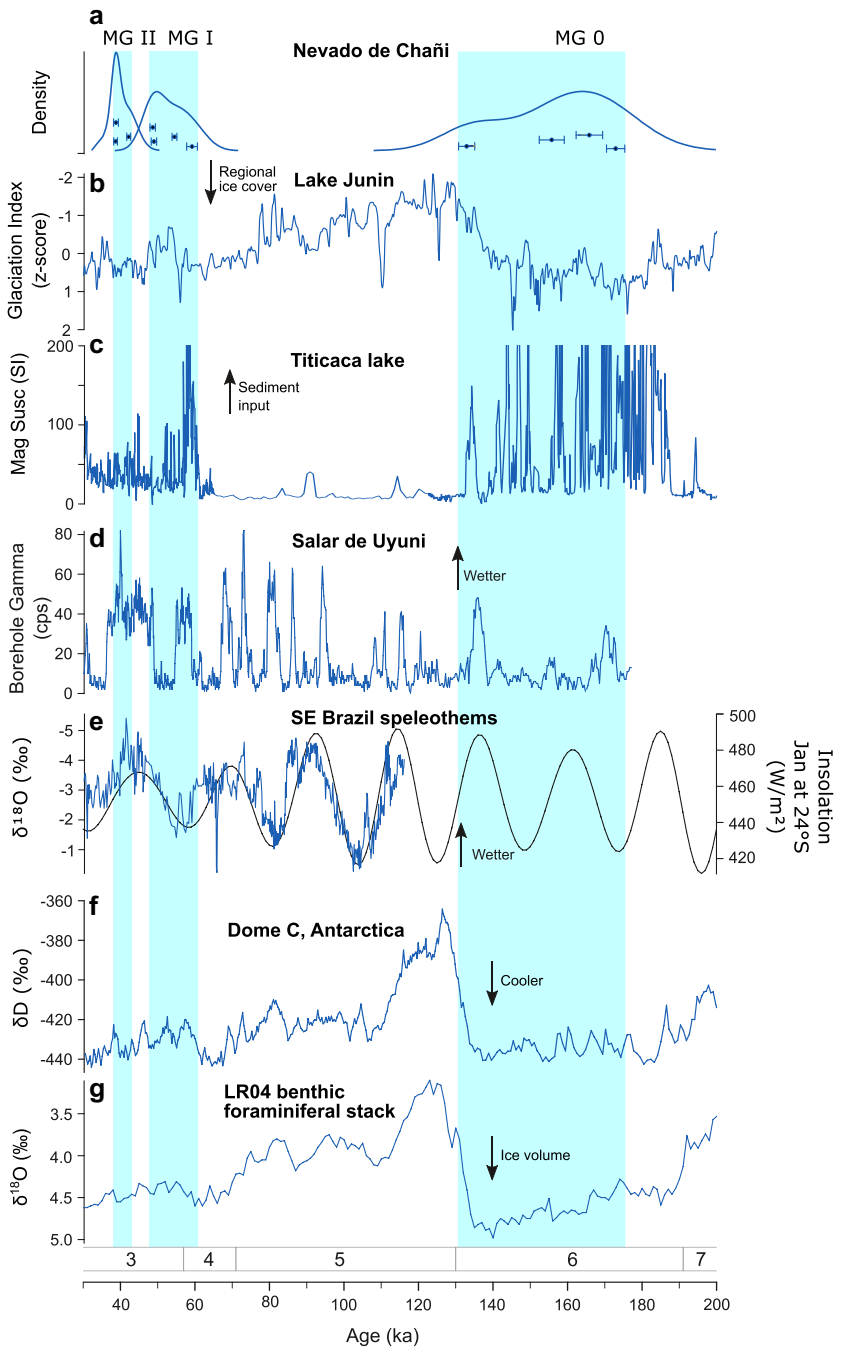

Figure 6. Nevado de Chañi pre-MIS 2 glacial chronology and selected paleoclimatic proxies (panels b–f are north to south; see Fig. 1 for location). (a) ^{10}Be ages (without outliers) and their kernel relative density estimates from Nevado de Chañi moraine groups (MG). Vertical blue bars indicate the chronology range from each MG. (b) Glaciation index from Lake Junin (Peruvian Andes, 11°S) as a proxy of the extent of regional ice-cover (Rodbell et al., 2022). (c) Magnetic susceptibility of Lake Titicaca (16°S) sediments as a proxy of surrounding Cordillera sediment input and regional glaciation (Fritz et al., 2007). (d) Natural gamma radiation of the Salar de Uyuni (20°S) drill core, which is a proxy for effective moisture (Fritz et al., 2004). (e) Stable oxygen isotope of Botuverá speleothem (27°S, Brazil) (Cruz et al., 2005) and January solar insolation at 24°S (Nevado de Chañi) (Laskar et al., 2004). (f) Deuterium record from the Antarctic Dome C (75°S) ice core as a proxy for mid-high latitude Southern Hemisphere temperature (EPICA, 2004). (g) The LR04 benthic foraminiferal stack of globally distributed records, which is largely a proxy of Northern Hemisphere ice volume (Lisiecki and Raymo, 2005), with Marine Isotope Stage (MIS) numbers at the bottom. [Color figure can be viewed at wileyonlinelibrary.com]

southern sector of the Andes, in Patagonia. In this region, the MIS 6 glacial activity is represented by one or probably two distinct events (Peltier et al., 2023; Leger et al., 2023). The European Ice Sheet also presents two different well-defined glacier advances (named Drenthe and Warthe) during MIS 6 (Toucanne et al., 2009; Wislon et al., 2021). Given the range of chronology of this glacial event (MG 0), the Nevado de Chañi record may contain either one long continuous expansion, or two distinct events within MIS 6 (see 'Glacier chronology' above) similar to the other sites in both hemispheres; additional data are needed to evaluate the detailed structure of MG 0.

Other tropical–subtropical proxy records spanning MIS 6 include the glaciation index from lake Junín (a proxy for clastic sediment flux and the extent of regional ice-cover) in the Andes of Peru at 11°S (Rodbell et al., 2022). High (positive) values indicate glacial conditions in phase with the period of MG 0 formation (Fig. 6). The lake sediment record from Uyuni in the Bolivian Altiplano shows that during MG 0 time the climate was predominately dry, but with short periods of wetter conditions (Fritz et al., 2004). Further evidence of regional glacial conditions is provided by the Lake Titicaca record that indicates a freshwater and higher-level paleolake during MIS 6; observations include carbonate-poor silts and clay with low calcium carbonate, high abundance of freshwater diatoms and high magnetic susceptibility (Fritz et al., 2007; 2012) (Fig. 6). Overall, low- to mid-latitude paleoclimatic proxies point to favorable conditions (cooler and wetter) for glacier expansions during MIS 6, in agreement with the MG 0 chronology at Nevado de Chañi massif.

During MIS 5 (130–71 ka), which includes the last interglacial period (5e), no glacial activity is documented around Nevado de Chañi (Fig. 6). If glaciers existed, they were less extensive than those corresponding to MG I or II. Glacier activity in the Central Andes was almost absent during MIS 5 (D'Arcy et al., 2019). Likewise, the Lake Junin glaciation index exhibits low (mostly negative) values (Fig. 6), evidencing that adverse conditions for glaciation existed in the region. Lake

© 2024 John Wiley & Sons, Ltd.

10991417, 0, Downloaded from https://onlinelibrary.wiley.com/doi/10.1002/jqs.3687 by Columbia University Health Sciences, Wiley Online Library on [14/01/2025]. See the Terms and Conditions (https://onlinelibrary.wiley.com/terms-and-conditions) on Wiley Online Library for rules of use; OA articles are governed by the applicable Creative Commons License

Titicaca shows moments of high salinity denoting episodes of lake reduction and therefore a dry climate (Fritz et al., 2007, 2012). On the other hand, Salar de Uyuni sediments record several short-lived intervals of wetter conditions during MIS 5 (Fritz et al., 2004) suggesting that, even if humid periods occurred in the region, temperatures were not low enough to support glaciers. In this sense, temperature reconstructions from subtropical lowlands of southeast Brazil reveal that MIS 5 was warmer than MIS 6 (Rodriguez-Zorro et al., 2020). Over the Central Andes, glaciers were not extensive throughout MIS 5 despite at times some of the wettest conditions and temperatures perhaps not much higher than other periods during the last glacial cycle (Fig. 6).

Glacier activity returned to Nevado the Chañi around the MIS 4/3 transition and perhaps late in MIS 4, with ^{10}Be ages from ~59 to 49 ka, represented by MG I on both sides of the massif. That is, as surface exposure cosmogenic ages may reflect close to moraine abandonment, the oldest ages in the distribution may reflect a late MIS 4 glaciation. Subsequently, a glacier advance occurred during MIS 3, between ~42 and ~39 ka, with MG II as evidence. Interestingly, MG II is only documented on the west side, being absent (so far) on the east side of Nevado de Chañi. After the MIS 4–3 glacier advances, a moraine-building event is recorded by MG III during MIS 2 or the global LGM. MG III marks an important glacier advance on the east side of the massif, which was less extensive (or even absent in some valleys) on the west side (Fig. 2). We suggest that on the east side of Nevado de Chañi the MG III event was slightly more extensive than the MG II event obliterating depositional evidence, which explains the absence of MG II on the eastern side of the massif.

The Nevado de Chañi MG I and II events coincided with other glacier records constrained with cosmogenic surface exposure dating in the Central Andes. For instance, in the nearby Puna region, lateral moraines from Quevar and Quirón sites (24°S) exhibit ages between 52 and 40 ka ($n = 5$) (Luna et al., 2018). Moraines (Stage II) from Chajnantor Plateau (Chilean Altiplano, 23°S) formed between 60 and 45 ka ($n = 4$) (Ward et al., 2015). Based on the oldest age of moraine M1, D'arcy et al. (2019) interpreted that the most external moraines of Sierra de Aconquija (27°S) were deposited at ~40 ka. In the Bolivian Altiplano, the oldest moraines (M1) from Uturuncu volcano (22°S) present scattered ages that range between ~65 and 37 ka ($n = 6$) (Blard et al., 2014). Glacier activity matching the MG II chronology, which is only dated on the west side of the massif, is also found elsewhere in the southern Central Andes, south to the Arid Diagonal (e.g. Zech et al., 2007; Aguilar et al., 2022; Garcia et al., 2024). In consonance with our results, world-wide reviews of cosmogenic surface exposure dating indicate that many glacier systems were more extensive during MIS 4 (and MIS 3) compared with those corresponding to MIS 2 (Hughes et al., 2013; Doughty et al., 2021). Our study also adds to a growing body of evidence for large MIS 3 glaciations throughout South America and the Southern Hemisphere (e.g. Denton et al., 2021).

A period of intense glacier activity in the Peruvian Andes (high values of glaciation index; Rodbell et al., 2022) is coincident with MG I and II chronology. The Altiplano lakes record two periods of higher lake level and wetter conditions during MIS 4 and 3 partially matching with the MG I and II chronologies (Fig. 6). The Uyuni salt-lake turned into a long-lived shallow and salty lake between ~60 and 55 ka, and a long-lived shallow lake between ~46 and 36 ka (Baker and Fritz, 2015), whereas Lake Titicaca shows moments of fresher and deeper conditions. Close to Nevado de Chañi, in the Laguna La Salada (23°S), a deep and often stratified paleolake stage was reconstructed during the period just prior to ~34 ka (Guerra et al., 2022).

In sum, from a broad perspective the glacier activity prior to the global LGM around Nevado de Chañi is well correlated with low-latitude records, cold conditions and periods of high Northern Hemisphere ice volume, and low Antarctic (i.e. high latitude) temperature. More glacier activity recorded by the glaciation index in Lake Junin, together with other regional lake and glacier expansions in the Central Andes, is in agreement with the reconstructions around the Nevado de Chañi massif (Fig. 6). Thus, there is a strong link between tropical and subtropical (Cordillera Oriental) records along the Andes, which in turn are in phase with Northern Hemisphere glacial conditions (MIS 6, 4–3 and 2). We hypothesize that glacier expansions around and just after the MIS 4/3 transition could be analogies to those around the MIS 2/1 boundary, that is after the maximum ice volume/sea level low (e.g. Tauca phase – Heinrich stadial 1 time) (Martini et al., 2017a; Mey et al., 2020).

Paleoclimatic context

Collectively, records show that multimillennial climate changes that drive glacier expansions in the Central Andes would have involved the SASM system variability and intensity, controlling the hydrological systems in the subtropical Andes. Since at least MIS 6, the intensification of the SASM would have led to strengthening of the South America Low Level Jet, increasing the moisture transport from the Amazon region into northwestern Argentina and Cordillera Oriental, leading to glacier expansions at Nevado de Chañi during moments of high Northern Hemisphere ice volume. This indicates that during periods of glacier expansions a combination of wetter and cooler conditions (i.e. global glacial maxima) prevailed, which is also in agreement with glacial and hydrological modeling studies throughout the last glacial termination in the subtropical Andes (Placzek et al., 2013; Martin et al., 2018; Mey et al., 2020). Furthermore, when cloudy (i.e. wetter), this could have reduced substantially the impact of shortwave radiation on sublimation received at such high elevations (>4000 m asl) and dry climate (Vargo et al., 2018). Cooling during global glaciation maxima could have involved, in addition, cold fronts that reached the Cordillera Oriental from the south (e.g. Marengo and Rogers, 2001; Garreaud et al., 2009).

To explore further past glacial–climate drivers in the subtropical Andes, we compared the lake and glacial activity with cave records from eastern Brazil, closer to the Atlantic Ocean, which show strong precessional modulated signals (Cruz et al., 2005) (Fig. 6). Over at least the past ~300 ka precessional-scale insolation variations have impacted the intensity of the SASM and its components, producing major hydroclimate changes in the Amazonas and Central Andes superposed on shorter (millennial-scale) fluctuations (Cheng et al., 2013; Baker and Fritz, 2015; Burns et al., 2019; Hou et al., 2020). For comparison, glacier and lake records in the Cordillera Oriental and Altiplano of the Central and tropical Andes sometimes are in phase with lows and other times with highs in precessional insolation (see MG I and II chronology on Fig. 6). That is, caves far east of the Andes more clearly record a strong precessional precipitation signal compared with glacier records. By contrast, glaciers in the high Andes are also sensitive to temperature reduction in addition to precipitation, suggesting that glaciers are not exclusively a proxy of SASM precipitation. In this sense, during the warmer MIS 5 the Botuverá speleothem record shows the precipitation signal in consonance with the insolation precession cycles, exhibiting two clear periods of high precipitation (Fig. 6). Nevertheless, no glacial activity was recorded in the Nevado de Chañi or the Central Andes. Indeed, the MIS 5 precessional

© 2024 John Wiley & Sons, Ltd.

10991417, 0, Downloaded from https://onlinelibrary.wiley.com/doi/10.1002/jqs.3687 by Columbia University Health Sciences, Wiley Online Library on [14/01/2025]. See the Terms and Conditions (https://onlinelibrary.wiley.com/terms-and-conditions) on Wiley Online Library for rules of use; OA articles are governed by the applicable Creative Commons License

cycles may have been even slightly wetter than those from MIS 4 to 2. Yet, these high MIS 5 precipitation increases were not enough to cause glacier advances, which also require reduced temperatures, as occurred during MIS 6, and MIS 4 to 2. Therefore, we conclude that glacial expansions in the Central Andes may have occurred under wetter conditions and during Northern Hemisphere or global glaciations when temperatures were reduced.

Conclusions

The Nevado de Chañi presents a rich history of Late Pleistocene glaciations. Our study reveals that three main pre-MIS 2 moraine groups are preserved around the massif, which represent different periods of widespread glacier expansions. The different moraine group landforms show contrasting glacier expansions between both sides (east and west) of the massif. MG 0 is the most expanded glacial event preserved and has been dated to between ~173 and ~134 ka, in phase with MIS 6. Afterwards, no glacial activity was recorded during MIS 5, despite at times high precipitation recorded in other Andean records and cave speleothems to the east in the lowlands. Renewed glacial expansions occurred during MIS 4–3 and 3 represented by MG I (~59–49 ka) and MG II (~42–39 ka). Comparison of the glacier chronology with regional paleoclimate proxies in the central and low-latitude Andes highlights a strong correlation between glacial expansions and moments of regional and global glaciations, low Antarctic temperature, and Andean lake highstands. We conclude that collectively the lines of evidence suggest broad synchronicity of ice age conditions during the Late Pleistocene in the subtropical and tropical Andes. The multimillennial Nevado de Chañi record, and other records in the Central Andes and east of the Arid Diagonal, at times also show glacier advances since MIS 6 during regional wetter phases, probably driven by the intensification of the SASM and its components, such as the South America Low Level Jet, acting during periods of Northern Hemisphere and global cool intervals and glaciations. We posit that wet periods without significant temperature reductions are not enough to leave an imprint of glacier expansions in the subtropical Andes, as evident by the absence of such landforms during MIS 5 and other (warm and) wet periods.

Acknowledgments. This research was supported by SECYT-UNC (Proyecto Consolidar 2023), CONICET (PIBAA 28720210101267) and NSF EAR-2035479. We acknowledge support from a seed grant supported by an NSF grant to PRIME Lab, grant # 2300559. We thank Philip Hughes, Roland Zech and an anonymous reviewer for their valuable comments that helped to improve our work.

Data Availability Statement

The data that support the findings of this study are available from the corresponding author upon reasonable request.

Abbreviations. AMS, Accelerator Mass Spectrometry; GNSS, Global Navigation Satellite System; ITCZ, Intertropical Convergence Zone; LGM, Last Glacial Maximum; MG, Moraine group; MIS, Marine Isotope Stage; SASM, South American Summer Monsoon.

References

Aguilar, G., Riquelme, R., Lohse, P., Cabré A. & García J.-L. (2022) Chronology of glacial advances and deglaciation in the encierro river valley (29° Lat. S), Southern Atacama desert, based on geomorphological mapping and cosmogenic ^{10}be exposure ages. *Frontiers in Earth Science*, 10, 878318. https://doi.org/10.3389/FEART.2022.878318

Baker, P.A. & Fritz, S.C. (2015) Nature and causes of Quaternary climate variation of tropical South America. *Quaternary Science Reviews*, 124, 31–47. Available at: https://doi.org/10.1016/j.quascirev.2015.06.011

Baker, P.A., Rigsby, C.A., Seltzer, G.O., Fritz, S.C., Lowenstein, T.K., Bacher, N.P. et al. (2001) Tropical climate changes at millennial and orbital timescales on the Bolivian Altiplano. *Nature*, 409, 698–701. Available at: https://doi.org/10.1038/35055524

Balco, G., Stone, J.O., Lifton, N.A. & Dunai, T.J. (2008) A complete and easily accessible means of calculating surface exposure ages or erosion rates from ^{10}Be and 26Al measurements. *Quaternary Geochronology*, 3, 174–195. Available at: https://doi.org/10.1016/j.quageo.2007.12.001

Bianchi, A.R. & Cravero, S.A.C. (2010) Atlas climático digital de la República Argentina. https://inta.gob.ar/documentos/atlas-climatico-digital-de-la-republica-argentina

Bianchi, A.R. & Yañez, C.E. (1992) Las precipitaciones en el noroeste argentino. INTA Estación Experimental Agropecuaria, Salta, 393pp.

Blard, P.H., Lavé, J., Farley, K.A., Fornari, M., Jiménez, N. & Ramirez, V. (2009) Late local glacial maximum in the Central Altiplano triggered by cold and locally-wet conditions during the paleolake Tauca episode (17-15 ka, Heinrich 1). *Quaternary Science Reviews*, 28, 3414–3427. Available at: https://doi.org/10.1016/j.quascirev.2009.09.025

Blard, P.H., Lave, J., Farley, K.A., Ramirez, V., Jimenez, N., Martin, L.C.P. et al. (2014) Progressive glacial retreat in the Southern Altiplano (Uturuncu volcano, 22°S) between 65 and 14 ka constrained by cosmogenic ^{3}He dating. *Quaternary Research*, 82, 209–221. Available at: https://doi.org/10.1016/j.yqres.2014.02.002

Bromley, G.R.M., Schaefer, J.M., Hall, B.L., Rademaker, K.M., Putnam, A.E., Todd, C.E. et al. (2016) A cosmogenic ^{10}Be chronology for the local last glacial maximum and termination in the Cordillera Oriental, southern Peruvian Andes: Implications for the tropical role in global climate. *Quaternary Science Reviews*, 148, 54–67. Available at: https://doi.org/10.1016/j.quascirev.2016.07.010

Burns, S.J., Welsh, L.K., Scroxton, N. et al. (2019) Millennial and orbital scale variability of the South American Monsoon during the penultimate glacial period. *Scientific Reports 2019, 9:1* 9(1), 1–5. Available at: https://doi.org/10.1038/s41598-018-37854-3

Cheng, H., Sinha, A., Cruz, F.W., Wang, X., Edwards, R.L., d'Horta, F.M. et al. (2013) Climate change patterns in Amazonia and biodiversity. *Nature Communications*, 4(1), 1411. Available at: https://doi.org/10.1038/ncomms2415

Clark, P.U., Dyke, A.S., Shakun, J.D., Carlson, A.E., Clark, J., Wohlfarth, B. et al. (2009) The Last Glacial Maximum. *Science*, 325(1979), 710–714. Available at: https://doi.org/10.1126/science.1172873

Cruz F.W., J.r, Burns, S.J., Karmann, I., Sharp, W.D., Vuille, M., Cardoso, A.O. et al. (2005) Insolation-driven changes in atmospheric circulation over the past 116,000 years in subtropical Brazil. *Nature*, 434(7029), 63–66. Available at: https://doi.org/10.1038/nature03365

D'Arcy, M., Schildgen, T.F., Strecker, M.R., Wittmann, H., Duesing, W., Mey, J. et al. (2019) Timing of past glaciation at the Sierra de Aconquija, northwestern Argentina, and throughout the Central Andes. *Quaternary Science Reviews*, 204, 37–57. Available at: https://doi.org/10.1016/j.quascirev.2018.11.022

de Carvalho, L.M.V. & Cavalcanti, I.F.A. (2016) The South American Monsoon System (SAMS). Springer Climate 121–148. https://doi.org/10.1007/978-3-319-21650-8_6/COVER

Denton, G.H., Putnam, A.E., Russell, J.L., Barrell, D.J.A., Schaefer, J.M., Kaplan, M.R. et al. (2021) The Zealandia Switch: Ice age climate shifts viewed from Southern Hemisphere moraines. *Quaternary Science Reviews*, 257, 106771. Available at: https://doi.org/10.1016/J.QUASCIREV.2020.106771

Doughty, A.M., Kaplan, M.R., Peltier, C. & Barker, S. (2021) A maximum in global glacier extent during MIS 4. *Quaternary Science Reviews*, 261, 106948. Available at: https://doi.org/10.1016/j.quascirev.2021.106948

EPICA. (2004) Eight glacial cycles from an Antarctic ice core. Nature 429, 623–628. http://www.nature.com/nature/journal/v429/n6992/suppinfo/nature02599_S1.html

Fritz, S.C., Baker, P.A., Lowenstein, T.K., Seltzer, G.O., Rigsby, C.A., Dwyer, G.S. et al. (2004) Hydrologic variation during the last 170,000 years in the southern hemisphere tropics of South America. *Quaternary Research*, 61, 95–104. Available at: https://doi.org/10.1016/j.yqres.2003.08.007

© 2024 John Wiley & Sons, Ltd.

10991417, 0, Downloaded from https://onlinelibrary.wiley.com/doi/10.1002/jqs.3687 by Columbia University Health Sciences, Wiley Online Library on [14/01/2025]. See the Terms and Conditions (https://onlinelibrary.wiley.com/terms-and-conditions) on Wiley Online Library for rules of use; OA articles are governed by the applicable Creative Commons License

Fritz, S.C., Baker, P.A., Seltzer, G.O., Ballantyne, A., Tapia, P., Cheng, H. et al. (2007) Quaternary glaciation and hydrologic variation in the South American tropics as reconstructed from the Lake Titicaca drilling project. *Quaternary Research*, 68, 410–420. Available at: https://doi.org/10.1016/j.yqres.2007.07.008

Fritz, S.C., Baker, P.A., Tapia, P., Spanbauer, T. & Westover, K. (2012) Evolution of the Lake Titicaca basin and its diatom flora over the last ~370,000 years. *Palaeogeography, Palaeoclimatology, Palaeoecology*, 317–318, 93–103. Available at: https://doi.org/10.1016/J.PALAEO.2011.12.013

García, J.L., Carraha, J., Fernández-Navarro, H., Nussbaumer, S.U., Pérez, F., Hidy, A.J. et al. (2024) Glacial to periglacial transition at the end of the last ice age in the subtropical semiarid Andes. *Geomorphology*, 465, 109379. Available at: https://doi.org/10.1016/J.GEOMORPH.2024.109379

Garreaud, R.D., Vuille, M., Compagnucci, R. & Marengo, J. (2009) Present-day South American climate. *Palaeogeography, Palaeoclimatology, Palaeoecology*, 281, 180–195. Available at: https://doi.org/10.1016/j.palaeo.2007.10.032

Gillespie, A. & Molnar, P. (1995) Asynchronous maximum advances of mountain and continental glaciers. *Reviews of Geophysics*, 33, 311–364. Available at: https://doi.org/10.1029/95RG00995

González, M.A., Tchilinguirian, P., Pereyra, F. et al. (2004) Hoja Geológica 2366-IV Ciudad de Libertador General San Martín, provincias de Jujuy y Salta: SEGEMAR, scale 1:250.000, 1 sheet, 114 pp text.

Guerra, L., Martini, M.A., Vogel, H., Piovano, E.L., Hajdas, I., Astini, R. et al. (2022) Microstratigraphy and palaeoenvironmental implications of a Late Quaternary high-altitude lacustrine record in the subtropical Andes. *Sedimentology*, 69, 2585–2614. Available at: https://doi.org/10.1111/SED.13004

Hijmans, R.J., Cameron, S.E., Parra, J.L., Jones, P.G. & Jarvis, A. (2005) Very high resolution interpolated climate surfaces for global land areas. *International Journal of Climatology*, 25, 1965–1978. Available at: https://doi.org/10.1002/joc.1276

Hou, A., Bahr, A., Raddatz, J., Voigt, S., Greule, M., Albuquerque, A.L. et al. (2020) Insolation and Greenhouse Gas Forcing of the South American Monsoon System Across Three Glacial-Interglacial Cycles. *Geophysical Research Letters*, 47, e2020GL087948. Available at: https://doi.org/10.1029/2020GL087948

Hughes, P.D. (2022) Concept and global context of the glacial landforms from the Last Glacial Maximum. In: Palacios, D., Hughes, P.D., Ruiz, J.M.G., & Andrés, N.D. (eds.) *European glacial landscapes: maximum extent of glaciations*. Amsterdam: Elsevier. pp. 355–358. Available at: https://doi.org/10.1016/B978-0-12-823498-3.00039-X

Hughes, P.D. & Gibbard, P.L. (2015) A stratigraphical basis for the Last Glacial Maximum (LGM). *Quaternary International*, 383, 174–185. Available at: https://doi.org/10.1016/J.QUAINT.2014.06.006

Hughes, P.D., Gibbard, P.L. & Ehlers, J. (2013) Timing of glaciation during the last glacial cycle: Evaluating the concept of a global "Last Glacial Maximum" (LGM). *Earth-Science Reviews*, 125, 171–198. Available at: https://doi.org/10.1016/j.earscirev.2013.07.003

Kelly, M.A., Lowell, T.V., Applegate, P.J., Phillips, F.M., Schaefer, J.M., Smith, C.A. et al. (2015) A locally calibrated, late glacial ^{10}Be production rate from a low-latitude, high-altitude site in the Peruvian Andes. *Quaternary Geochronology*, 26, 70–85. Available at: https://doi.org/10.1016/j.quageo.2013.10.007

Laskar, J., Robutel, P., Joutel, F., Gastineau, M., Correia, A. C. M., & Levrard, B. (2004) A long-term numerical solution for the insolation quantities of the Earth. *Astronomy and Astrophysics*, 428. Available at: https://doi.org/10.1051/0004-6361:20041335

Leger, T.P.M., Hein, A.S., Rodés, Á., Bingham, R.G., Schimmelpfennig, I., Fabel, D. et al. (2023) A cosmogenic nuclide-derived chronology of pre-Last Glacial Cycle glaciations during MIS 8 and MIS 6 in northern Patagonia. *Climate of the Past*, 19, 35–59. Available at: https://doi.org/10.5194/CP-19-35-2023

Lisiecki, L.E. & Raymo, M.E. (2005) A Pliocene-Pleistocene stack of 57 globally distributed benthic δ ^{18} O records. Paleoceanography 20, *n*/a-*n*/a. https://doi.org/10.1029/2004PA001071

Luna, L.V., Bookhagen, B., Niedermann, S., Rugel, G., Scharf, A. & Merchel, S. (2018) Glacial chronology and production rate cross-calibration of five cosmogenic nuclide and mineral systems from the southern Central Andean Plateau. *Earth and Planetary Science Letters*, 500, 242–253. Available at: https://doi.org/10.1016/j.epsl.2018.07.034

Mackintosh, A.N., Anderson, B.M. & Pierrehumbert, R.T. (2017) Reconstructing Climate from Glaciers. *Annual Review of Earth and Planetary Sciences*, 45, 649–680. Available at: https://doi.org/10.1146/annurev-earth-063016-020643

Marengo, J.A. & Rogers, J.C. (2001) Polar air outbreaks in the Americas: assessments and impacts duringmodern and past climates. In: Markgraf, V. (ed.) *Interhemispheric climate linkages*. San Diego: Academic Press. pp. 31–51. Available at: https://doi.org/10.1016/B978-012472670-3/50006-9

Martin, L.C.P., Blard, P.-H., Lavé, J., Braucher, R., Lupker, M., Condom, T. et al. (2015) In situ cosmogenic ^{10}Be production rate in the High Tropical Andes. *Quaternary Geochronology*, 30, 54–68. Available at: https://doi.org/10.1016/j.quageo.2015.06.012

Martin, L.C.P., Blard, P.-H., Lavé, J., Condom, T., Prémaillon, M., Jomelli, V. et al. (2018) Lake Tauca highstand (Heinrich Stadial 1a) driven by a southward shift of the Bolivian High. *Science Advances*, 4, eaar2514. Available at: https://doi.org/10.1126/sciadv.aar2514

Martin, L.C.P., Blard, P.H., Lavé, J., Jomelli, V., Charreau, J., Condom, T. et al. (2020) Antarctic-like temperature variations in the Tropical Andes recorded by glaciers and lakes during the last deglaciation. *Quaternary Science Reviews*, 247, 106542. Available at: https://doi.org/10.1016/J.QUASCIREV.2020.106542

Martini, M.A., Kaplan, M.R., Strelin, J.A. et al. (2017a) Late Pleistocene glacial fluctuations in Cordillera Oriental, subtropical Andes. *Quaternary Science Reviews*, 171, 245–259. Available at: https://doi.org/10.1016/j.quascirev.2017.06.033

Martini, M.A., Strelin, J.A. & Astini, R.A. (2013) Inventario y caracterización morfoclimática de los glaciares de roca en la Cordillera Oriental Argentina (entre 22° y 25°S). *Revista Mexicana de Ciencias Geológicas*, 30, 569–581.

Martini, M.A., Strelin, J.A., Flores, E. et al. (2017b) Recent climate warming and the Varas rock glacier activity, Cordillera Oriental, Central Andes of Argentina. *GeoResJ*, 14, 67–79. Available at: https://doi.org/10.1016/j.grj.2017.08.002

Mey, J., D'Arcy, M.K., Schildgen, T.F., Egholm, D.L., Wittmann, H. & Strecker, M.R. (2020) Temperature and precipitation in the southern Central Andes during the last glacial maximum, Heinrich Stadial 1, and the Younger Dryas. *Quaternary Science Reviews*, 248, 106592. Available at: https://doi.org/10.1016/J.QUASCIREV.2020.106592

Mix, A. (2001) Environmental processes of the ice age: land, oceans, glaciers (EPILOG). *Quaternary Science Reviews*, 20, 627–657. Available at: https://doi.org/10.1016/S0277-3791(00)00145-1

Nishiizumi, K., Imamura, M., Caffee, M.W., Southon, J.R., Finkel, R.C. & McAninch, J. (2007) Absolute calibration of ^{10}Be AMS standards. *Nuclear Instruments and Methods in Physics Research Section B: Beam Interactions with Materials and Atoms*, 258, 403–413. Available at: https://doi.org/10.1016/j.nimb.2007.01.297

Olson, M. & Rupper, S. (2019) Impacts of topographic shading on direct solar radiation for valley glaciers in complex topography. *The Cryosphere*, 13, 29–40. Available at: https://doi.org/10.5194/TC-13-29-2019

Palacios, D., Stokes, C.R., Phillips, F.M., Clague, J.J., Alcalá-Reygosa, J., Andrés, N. et al. (2020) The deglaciation of the Americas during the Last Glacial Termination. *Earth-Science Reviews*, 203, 103113. Available at: https://doi.org/10.1016/J.EARSCIREV.2020.103113

Peltier, C., Kaplan, M.R., Sagredo, E.A., Moreno, P.I., Araos, J., Birkel, S.D. et al. (2023) The last two glacial cycles in central Patagonia: A precise record from the Ñirehuao glacier lobe. *Quaternary Science Reviews*, 304, 107873. Available at: https://doi.org/10.1016/J.QUASCIREV.2022.107873

Placzek, C.J., Quade, J. & Patchett, P.J. (2013) A 130 ka reconstruction of rainfall on the Bolivian Altiplano. *Earth and Planetary Science Letters*, 363, 97–108. Available at: https://doi.org/10.1016/j.epsl.2012.12.017

Rodbell, D.T., Hatfield, R.G., Abbott, M.B., Chen, C.Y., Woods, A., Stoner, J.S. et al. (2022) 700,000 years of tropical Andean glaciation. *Nature*, 607(7918), 301–306. Available at: https://doi.org/10.1038/s41586-022-04873-0

Rodríguez-Zorro, P.A., Ledru, M.P., Bard, E., Aquino-Alfonso, O., Camejo, A., Daniau, A.L. et al. (2020) Shut down of the South American summer monsoon during the penultimate glacial.

© 2024 John Wiley & Sons, Ltd.

10991417, 0, Downloaded from https://onlinelibrary.wiley.com/doi/10.1002/jqs.3687 by Columbia University Health Sciences, Wiley Online Library on [14/01/2025]. See the Terms and Conditions (https://onlinelibrary.wiley.com/terms-and-conditions) on Wiley Online Library for rules of use; OA articles are governed by the applicable Creative Commons License

Scientific Reports, 10, 6275. Available at: https://doi.org/10.1038/s41598-020-62888-x

Sagredo, E.A. & Lowell, T.V. (2012) Climatology of Andean glaciers: A framework to understand glacier response to climate change. *Global and Planetary Change*, 86–87, 101–109. Available at: https://doi.org/10.1016/j.gloplacha.2012.02.010

Schaefer, J.M., Denton, G.H., Kaplan, M., Putnam, A., Finkel, R.C., Barrell, D.J.A. et al. (2009) High-frequency Holocene glacier fluctuations in New Zealand differ from the northern signature. *Science*, 324(1979), 622–625. Available at: https://doi.org/10.1126/science.1169312

Toucanne, S., Zaragosi, S., Bourillet, J.F., Cremer, M., Eynaud, F., Van Vliet-Lanoë, B. et al. (2009) Timing of massive 'Fleuve Manche' discharges over the last 350 kyr: insights into the European ice-sheet oscillations and the European drainage network from MIS 10 to 2. *Quaternary Science Reviews*, 28, 1238–1256. Available at: https://doi.org/10.1016/J.QUASCIREV.2009.01.006

Vargo, L.J., Galewsky, J., Rupper, S. & Ward, D.J. (2018) Sensitivity of glaciation in the arid subtropical Andes to changes in temperature, precipitation, and solar radiation. *Global and Planetary Change*, 163, 86–96. Available at: https://doi.org/10.1016/J.GLOPLACHA.2018.02.006

Vera, C., Higgins, W., Amador, J., Ambrizzi, T., Garreaud, R., Gochis, D. et al. (2006) Towards a unified view of the American Monsoon System. *Journal of Climate*, 19, 4977–5000.

Viale, M., Bianchi, E., Cara, L., Ruiz, L.E., Villalba, R., Pitte, P. et al. (2019) Contrasting Climates at Both Sides of the Andes in Argentina and Chile. *Frontiers in Environmental Science*, 7, 69. Available at: https://doi.org/10.3389/fenvs.2019.00069

Ward, D.J., Cesta, J.M., Galewsky, J. & Sagredo, E. (2015) Late pleistocene glaciations of the arid subtropical Andes and new results from the Chajnantor Plateau, northern Chile. *Quaternary Science Reviews*, 128, 98–116. Available at: https://doi.org/10.1016/j.quascirev.2015.09.022

Wilson, G.P., Frogley, M.R., Hughes, P.D., Roucoux, K.H., Margari, V., Jones, T.D. et al. (2021) Persistent millennial-scale climate variability in Southern Europe during Marine Isotope Stage 6. *Quaternary Science Advances*, 3, 100016. Available at: https://doi.org/10.1016/J.QSA.2020.100016

Woods, A., Rodbell, D.T., Abbott, M.B., Hatfield, R.G., Chen, C.Y., Lehmann, S.B. et al. (2020) Andean drought and glacial retreat tied to Greenland warming during the last glacial period. *Nature Communications*, 11, 5135. Available at: https://doi.org/10.1038/s41467-020-19000-8

Zappettini, E.O., Coira, B. & Santos, O.J. (2008) Edad U/Pb de la Formación Chañi: un granito del arco magmático Tilcárico, in: 17 Congreso Geológico Argentino, Abstractas I: 248-249.

Zech, J., Terrizzano, C., García-Morabito, E., Veit, H. & Zech, R. (2017) Timing and extent of late pleistocene glaciation in the arid Central Andes of Argentina and Chile (22°-41°S). *Cuadernos de Investigación Geográfica*, 43, 697–718. Available at: https://doi.org/10.18172/CIG.3235

Zech, J., Zech, R., Kubik, P.W. & Veit, H. (2009) Glacier and climate reconstruction at Tres Lagunas, NW Argentina, based on ^{10}Be surface exposure dating and lake sediment analyses. *Palaeogeography, Palaeoclimatology, Palaeoecology*, 284, 180–190. Available at: https://doi.org/10.1016/j.palaeo.2009.09.023

Zech, R., Kull, C., Kubik, P.W. & Veit, H. (2007) Exposure dating of Late Glacial and pre-LGM moraines in the Cordon de Doña Rosa, Northern/Central Chile (~31°S). *Climate of the Past*, 3, 1–14. Available at: https://doi.org/10.5194/CP-3-1-2007

Zhou, J. & Lau, K.M. (1998) Does a monsoon climate exist over South America? *Journal of Climate*, 11, 1020–1040. Available at: https://doi.org/10.1175/1520-0442(1998)011<1020:DAMCEO>2.0.CO;2

© 2024 John Wiley & Sons, Ltd.

10991417, 0, Downloaded from https://onlinelibrary.wiley.com/doi/10.1002/jqs.3687 by Columbia University Health Sciences, Wiley Online Library on [14/01/2025]. See the Terms and Conditions (https://onlinelibrary.wiley.com/terms-and-conditions) on Wiley Online Library for rules of use; OA articles are governed by the applicable Creative Commons License